WIND GENERATION SYSTEM FOR CHARGING BATTERIES

Isaac R. Machado[1], Herminio M. Oliveira F.[2], Luiz H. S. C. Barreto[2], and Demercil S. Oliveira Jr.[2]

[1]Federal University of Rio de Janeiro – COPPE/UFRJ
Laboratory of Power Eletronics
PO Box 68504, P.Code 21945-970, Tel.:+55(21)25628634
Rio de Janeiro-RJ – Brazil

[2]Federal University of Ceará – UFC
Group of Energy Processing and Control – GPEC
PO Box 6001, P.Code 60455-760, Tel.: +55(85)33669586
Fortaleza-CE – Brazil

isaac@coe.ufrj.br, demercil@dee.ufc.br, lbarreto@dee.ufc.br

***Abstract* – This paper is concerned with the study of a small size wind generation system for charging battery. A topology that aims at the exploitation of the energy generated at low speed is proposed. The characteristics of the wind turbine and the generator are discussed, providing the overview of the system modeling. Simulation tests of the system are obtained using MATLAB/SIMULINK, as the relevant results are supposed to be compared with experimental data and validate the proposal. The battery charging control is based on the checking the battery bank voltage and a protection against high wind speed is implemented through the limitation of the load current. The overall system supervision and verification of the analog parameters are performed using microcontroller PIC 16F876.**

***Keywords* – Battery charging, maximum power point operation, wind generation.**

NOMENCLATURE

B Coefficient of viscous friction (0.00467 Nm/rad/s);
$C_1, C_2, C_3, C_4, C_5, C_6$ Aerodynamic wind turbine constants.
E_a, E_b, E_c Induced electromotive force;
I_a, I_b, I_c Phase currents;
J Inertia moment (J=0.065 kg.m^2);
P Number of pole pairs (P=7);
Te Electrical torque;
T_m Mechanical torque;
ρ Differential operator;
ω_g Mechanics speed of the wind turbine;
θ_g Angle that defines the mechanical position of the rotor (rad);
θ_r Angle that defines the electrical position of the rotor (rad).

I. INTRODUCTION

A wind generation system can be used basically in three distinct applications: isolated systems, hybrid systems, and grid connected systems. Basic characteristics of the systems include power and energy storage capability. Generally, small size isolated systems demand energy storage, by the use of batteries or in the form of gravitational potential energy in order to store the water pumped in reservoirs raised for posterior use. More specifically, for electric generation in isolated systems, small wind turbines (400 W – 5 kW) for battery charging are very useful.

However, cost effectiveness is very important for such applications and topologies used for higher power generation are not viable [7] [8]. The direct connection of a three-phase diode controlled rectifier to the batteries is a common practice adopted by some manufactories [1]. Although there is simplicity and robustness, several problems associated with this solution result. Then, dc/dc converters have to be connected in series with the rectifier in order to adapt the generator voltage to the battery bank voltage. In [9-11], boost and buck-boost converters are used. However, in such architectures, a dc-dc converter rated at full power has to be used, what increases cost, mainly considering the sites where low speed winds are the more common. Then, this paper proposes an arrangement that employs a dc-dc converter to be used for low speed range. For higher speeds, the rectifier is supposed to feed the battery directly.

II. PROPOSED TOPOLOGY

A. Power Circuit

The studied system is available commercially and manufactured by ENERSUD manufacturer [1]. It is composed of a wind turbine directly connected to a permanent magnet synchronous generator (PMSG) without gear box. A three-phase full-bridge rectifier supplies the battery bank directly, which is composed of two batteries (MOURA CLEAN model 12MC150 – 12 V/150 Ah). This system is also available with the absence of charging controller, reducing the useful life of the batteries. Another limitation is the partial exploration of the available wind energy at low speed. This limitation is due to the direct connection of the batteries to three-phase rectifier. Therefore the presence of diodes does not allow for the energy transfer while the induced voltage does not exceed the battery voltage, what corresponds to approximately 270 rpm.

To solve these problems, a new topology is proposed, where a boost converter, a buck converter, and a three-phase bridge rectifier are connected in parallel. At low speed, the boost converter is used to draw the current from the generator to the batteries. When voltage V_{dc1} (Fig. 1) is greater than 25 V (high speed operation), the rectifier starts supplying energy directly to the batteries, as the converter is not operating. At low speeds (ωg<312rpm), the system operates in an optimum point. Maximum power point tracking (MPPT) is implemented with the average current mode control applied to the boost converter and based on curves obtained by simulations.

The buck converter has two functions: to perform speed reduction when requested or to limit the charging current, which occurs through the implementation of the input voltage control mode applied to the buck converter.

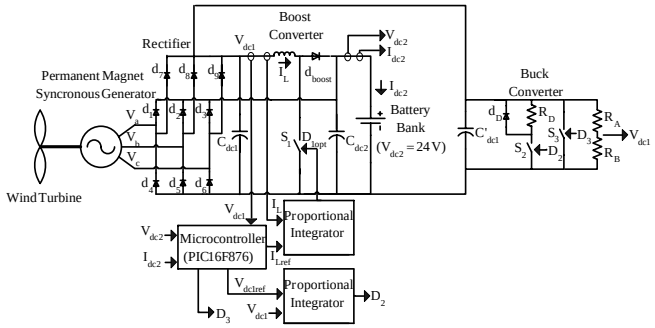

Fig. 1. Proposed topology.

B. Control Technique

The process is commanded by Microchip® microcontroller PIC16F876. The main functions of the microcontroller are:

• Determination the on/off state of the converters in accordance with the variations of wind speed (activation of shutdown function - SG 3525);

• Generation of the reference current I_{Lref}, for the average current mode control (boost converter) and reference voltage V_{dc1ref} for the voltage mode control (buck converter);

• Measurement of voltage $\boldsymbol{V_{dc2}}$ (charging controller) and current $\boldsymbol{I_{dc2}}$ (protection against overcurrent and overvoltage) of the battery bank).

• Signaling of the batteries charging level (leds).

The MPPT algorithm is based on the measurement of voltage $\boldsymbol{V_{dc1}}$ to generate the reference current $\boldsymbol{I_{Lref}}$, used in the average current mode control applied to the boost converter. Thus, for each input voltage ($\boldsymbol{V_{dc1}}$), the reference current is generated ($\boldsymbol{I_{Lref}}$), determining the optimum impedance seen from the generator terminals. The optimum reference currents are generated by the microcontroller, based on the simulation results presented in section IV.

The speed reduction process is set in the following cases:

• At each 10 minutes, voltage V_{dc2} is measured by the A/D converter and adopted as a reference for the determination of the battery charging level. In this case, the speed reduction is partial so that the charging stops and the open-circuit voltage is measured. Thus, if the complete charging is achieved, the turbine is fully stopped (by turning on switch S3) until uncharged batteries are connected;

• When requested by the user pushing an external button. This possibility is implemented for safety or maintenance purposes;

• When load current I_{dc2} reaches is maximum at 30 A (maximum current recommended by the battery manufacturer). In this case, speed reduction is partial and voltage V_{dc1} is decreased until I_{dc2} reaches less than 20 A;

• When voltage V_{dc2} reaches a maximum values up to 28.8 V (the maximum value recommended by the battery manufacturer is 14.4 V). In this case, speed reduction is partial and occurs until voltage $\boldsymbol{V_{dc1}}$ reaches 24 V.

III. SYSTEM MODELING

A. Wind Turbine Performance

An amount of wind mass m and density ρ_a that flows with speed u in the axial direction of the wind turbine has some kinetic energy. The available wind power P_v is the derivative of the kinetic energy with regard to time, given by equation (1):

$$P_v = \frac{1}{2}\cdot \rho_a \cdot A_v \cdot u^3 \tag{1}$$

The extracted mechanical power $\boldsymbol{P_m}$ from the available wind power $\boldsymbol{P_v}$ is determined by the power coefficient $\boldsymbol{C_p}$, according to equation (2).

$$P_m = C_p \cdot P_v = C_p \cdot \left(\frac{1}{2}\cdot \rho_a \cdot A_v \cdot u^3\right) \tag{2}$$

The performance of the power coefficient in wind turbines is determined by manufacturers through tests carried out in wind tunnels. The value of $\boldsymbol{C_p}$ is a function of the wind speed $\boldsymbol{u}$, rotation speed of the turbine $\boldsymbol{\omega_g}$, pitch angle $\boldsymbol{\beta}$, and the aerodynamic characteristics of the turbine.

The curve of the power coefficient for a given wind turbine is presented in equation (3):

$$C_p = C_1 \cdot \left(\frac{C_2}{\lambda_i} - C_3 \cdot \beta - C_4\right) \cdot e^{\frac{C_5}{\lambda_i}} + C_6 \cdot \lambda \tag{3}$$

Where constants $\boldsymbol{C_1}$ to $\boldsymbol{C_6}$ are parameters that depend on the wind turbine aerodynamic and $\boldsymbol{\lambda_i}$ is a parameter given in (4).

$$\frac{1}{\lambda_i} = \frac{1}{\lambda + 0.08.\beta} - \frac{0.035}{\beta^3 + 1} \tag{4}$$

In the simulation tests, the following values for the constants mentioned in equation (3) are considered:

$C_1 = 0.5176$, $C_2 = 116$, $C_3 = 0.40$, $C_4 = 5$, $C_5 = 21$, $C_6 = 0.0068$

These values are given for a three-bladed wind turbine, with similar aerodynamic characteristics to the turbine used in the system. The value of $\boldsymbol{\beta}$ chosen for simulation is 3º.

B. Generator Characteristics

The electrical machine used in the system is a permanent magnet synchronous generator (PMSG) rated at 1 kW, 1000 rpm, 7 pole pairs and axial flux. This type of machine is particularly interesting for applications in wind generation due to its inherent characteristics. Several studies such as those in [2] and [3] deal with the characteristics of this machine. The dynamic model of the machine is obtained in [3], described by expressions (5) to (8).

$$T_e = \frac{E_a \cdot I_a + E_b \cdot I_b + E_c \cdot I_c}{\omega_g} \tag{5}$$

$$J \cdot \rho \cdot \varpi_g = T_m - T_e - B \cdot \varpi_g \tag{6}$$

$$\rho \cdot \theta_g = \omega_g \tag{7}$$

$$\rho \cdot \theta_r = P \cdot \omega_g \tag{8}$$

The electrical model of the synchronous generator in steady-state operation is described by equation (9).

$$\begin{pmatrix} V_a \\ V_b \\ V_c \end{pmatrix} = \begin{pmatrix} E_a \\ E_b \\ E_c \end{pmatrix} - \begin{pmatrix} R_a & 0 & 0 \\ 0 & R_b & 0 \\ 0 & 0 & R_c \end{pmatrix} \begin{pmatrix} I_a \\ I_b \\ I_c \end{pmatrix} - \begin{pmatrix} L_a & M_{ab} & M_{ac} \\ M_{ba} & L_b & M_{bc} \\ M_{ca} & M_{cb} & L_c \end{pmatrix} \cdot \partial \begin{pmatrix} I_a \\ I_b \\ I_c \end{pmatrix} \tag{9}$$

To determine the physical parameters of the machine such as phase resistance (R_a, R_b, R_c), self-inductance (L_a, L_b, L_c) and mutual inductance (M_{nm}), several evaluation tests are performed as in [2]. The values considered in the simulation are 0.5 Ω/phase (resistance), 3.35 mH (self-inductance), and 3.06 mH (mutual inductance).

IV. SYSTEM SIMULATION

The system model is obtained considering the expressions presented in the previous session. Simulation tests are performed using MATLAB/SIMULINK.

The simulations have the objective to prove and to validate the existence of an optimum point of operation and to predict the behavior system for each wind speed. In a first moment a controlled voltage source was connected to the rectifier output. The controlled voltage source determines the linear variation of the output voltage from 0 to 70 V during 10 seconds, simulating a variation of the impedance seen from the generator. Then, for a wind speed of 7 m/s, the variation of the output impedance determines the variation of the generated voltage and mechanical speed (0 to 653 rpm in 10s).

The dynamic of the output power is verified in Fig. 2. Maximum power point is observed at 6.25 seconds, instant in which the output voltage reaches 44.1 V (optimum output voltage). Then, an optimum output voltage can be found for each wind speed.

The power coefficient is also an important parameter to be observed and is shown in Fig. 3. The performance of C_p is analyzed for the same described conditions in Fig. 2. It is important to notice that the output power waveform is similar to the power coefficient curve, however the maximum point occurs at different instants due to the internal losses in the machine and the diodes. The I^2R losses are responsible for great part of the internal losses in this type of machine.

The simulations are performed for some wind speeds (3 m/s to 10 m/s), as shown in Tables I and II. Although in Table I the obtained power coefficient is greater than in Table II, the output power obtained in Table II is greater than that Table I. For example, for u=10 m/s, the ouput power is about 638 W since V_{dc2} is maintained constant. If Vdc2 operates in the maximum power point, the output power becomes 1100 W, as the increase is 58%.

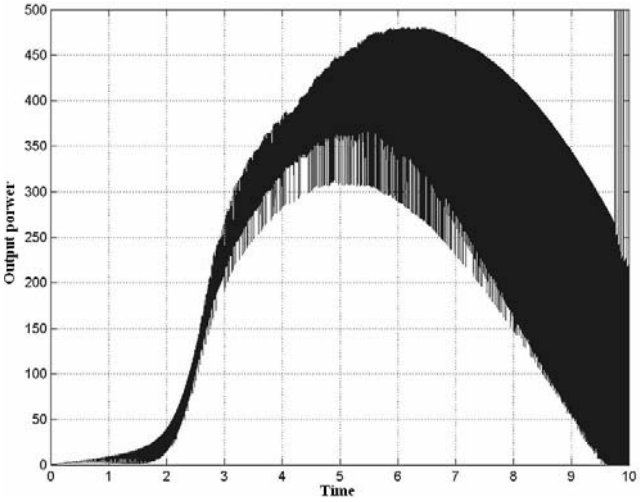

Fig. 2. Output power versus time for wind speed of 7 m/s and output voltage variation from 0 to 70V (simulation).

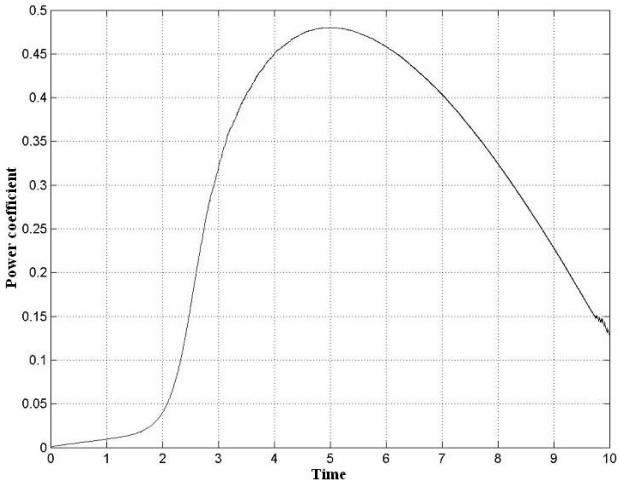

Fig. 3 Power coefficient versus time for wind speed of 7 m/s and output voltage variation from 0 to 70V (simulation).

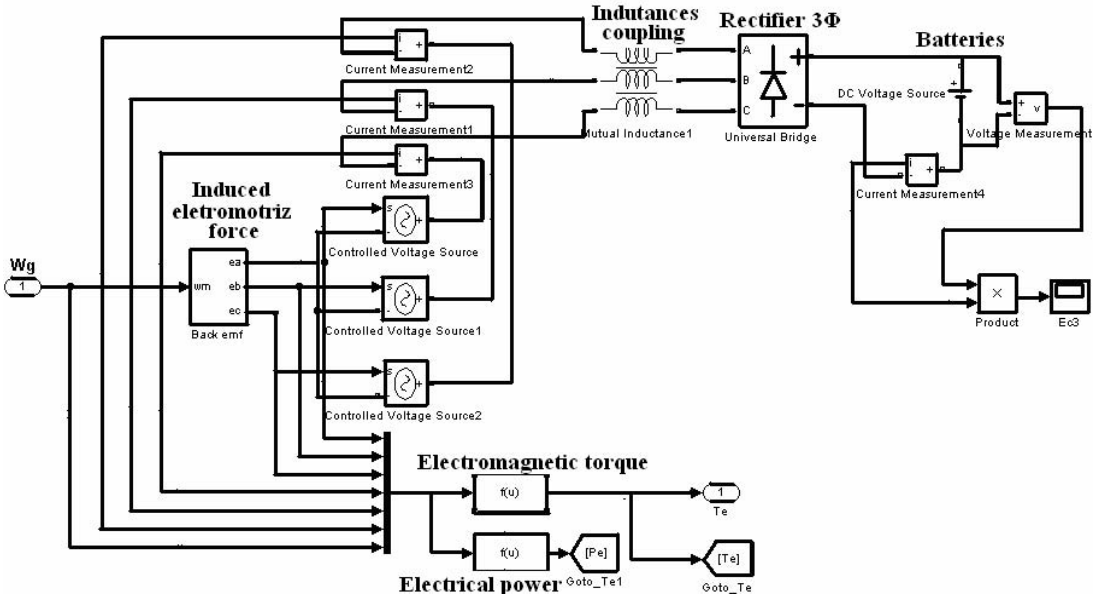

Fig. 4. Simulation schematic.

TABLE I
Simulation Results for Constant Output Voltage (24 V).

u (m/s)	V_{dc1} (V)	P_{dc1} (W)	I_{dc1} (A)	ω_g (rpm)	Cp	I_{ef} (A)	I^2R Loss (W)
3	24	21.6	0.9	271	0.181	0.75	0.84
4	24	69.6	2.9	298	0.474	2.35	8.28
5	24	144	6	325	0.471	4.5	30.37
6	24	218	9.1	364	0.479	7.3	79.93
7	24	268	11.2	405	0.479	9.2	126.96
8	24	408	17	450	0.476	13	253.5
9	24	528	22	501	0.479	17.5	459.3
10	24	638	26.6	558	0.472	22	726
11	24	852	35.5	623	0.473	26.1	1021.8
12	24	960	40	695	0.475	31	1441

TABLE II
Simulation Results for Maximum Power Point Operation.

u (m/s)	Optimum V_{dc1} (V)	P_{dc1} (W)	I_{dc1} (A)	ω_g (rpm)	Cp	I_{ef} (A)	I^2R Loss (W)
3	18	36.75	2.05	208	0.447	1.57	3.69
4	26.2	78.6	3	271	0.458	2.7	10.93
5	31	164.3	5.3	333	0.454	4.4	29.04
6	37.25	272.6	7.3	409	0.430	6.4	61.44
7	44.1	413.6	9.3	493	0.448	7.65	87.78
8	47.2	604.1	12.8	554	0.439	10.3	160.68
9	53	829.4	15.6	636	0.437	12.5	234.37
10	57	1100.1	19.3	708	0.432	15.2	360.37
11	61.5	1414.5	23	786	0.432	18.1	494.13
12	66	1773.4	26.8	866	0.426	21	661.5

Fig. 5 shows the simulated power curve and the manufacturer power curve for operation with constant output voltage equal to 24 V. The validation of the simulation is made by the comparison of the two curves. The proximity between the two curves is evident along the complete operation range, what is enough to validate the model.

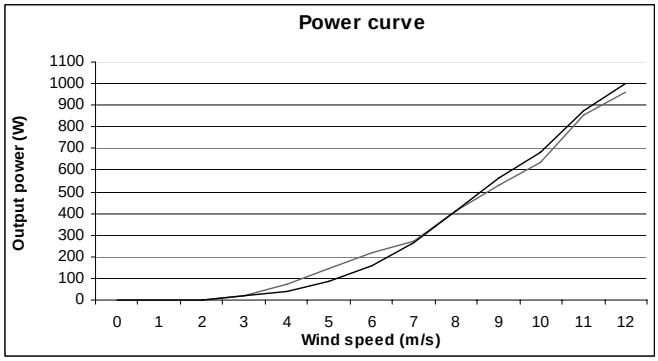

Fig. 5. Power curve (a – simulated, b – manufacturer).

V. EXPERIMENTAL RESULTS

In the new topology proposed here, a boost converter was introduced in order to improve the power generation at low wind speeds. The boost converter is designed for the operation in the range from 0 to about 70 W, according to Table II. The main rectifier is designed according to the specifications for v=12 m/s (see Table I). The experimental results were obtained for mechanical speeds of 269 rpm and 470 rpm. The boost converter becomes inoperative when voltage V_{dc1} reaches 25 V, as the battery bank is supplied directly by the three-phase rectifier.

Fig. 6 shows the generated phase voltage and the line current for mechanical speed of 269 rpm.

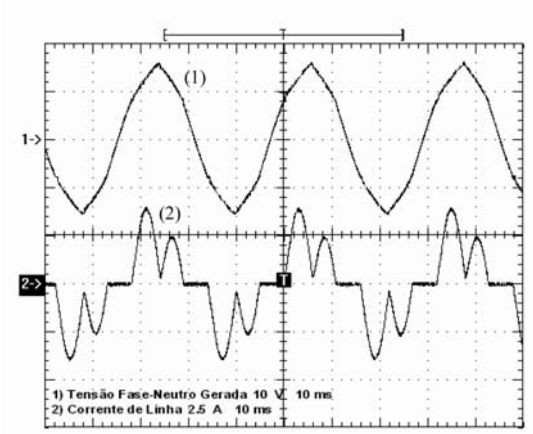

Fig. 6. (1) – Phase voltage (10 V/div. and 10 ms/div) and (2) - Line current (2.5 A/div. and 10 ms/div) at 269 rpm.

In this case, the rms value of the phase voltage is 10.36 V. The line current waveform is pulsed, which is identical to simulation result, and the rms value is 1.95 A. Therefore the input apparent power is 61.82 VA and the input active power is 50 W, and the machine power factor is 0.81. Fig. 7 shows the duty cycle and boost inductor current.

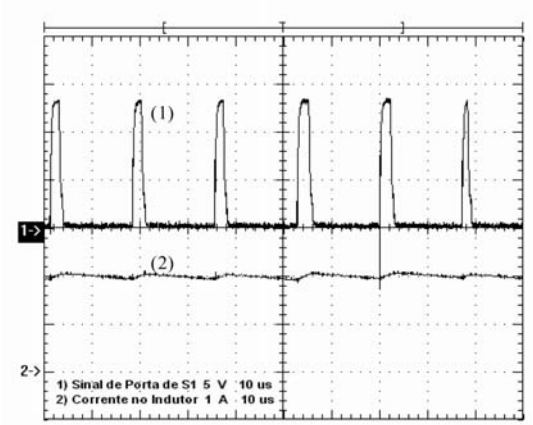

Fig. 7. (1) – Duty cycle, D_{opt} (5 V/div. and 10 µs/div) and (2) - Boost inductor current, I_L (1 A/div. and 10 µs/div) at 269 rpm.

The high frequency current ripple observed was 0.15 A and is in agreement with the design specifications (0.15 A). The average inductor current is 2 A and the switching frequency is 52 kHz.

Fig. 8 shows input voltage V_{dc1} across the boost converter for mechanical speed of 269 rpm. The voltage ripple is 2 V and is in agreement with the design specifications (10.15 V). Fig. 9 shows the battery bank voltage V_{dc2} and charging current I_{dc2} for mechanical speed of 269 rpm.

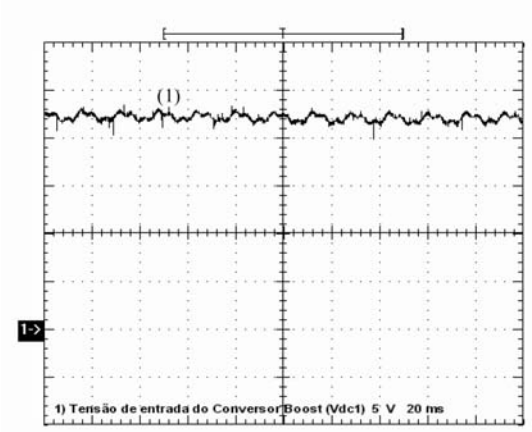

Fig. 8. (1) – Boost converter input voltage, V_{dc1} (5 V/div. and 20 ms/div) at 269 rpm.

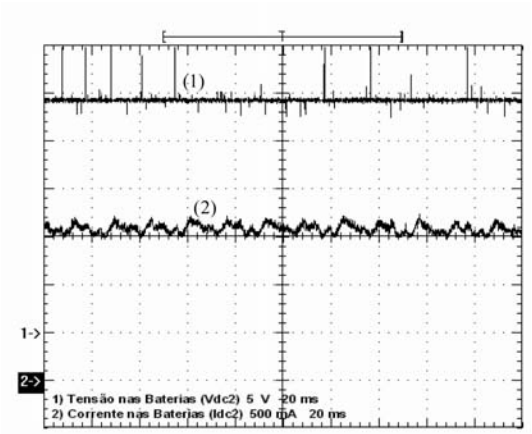

Fig. 9. (1) – Battery bank voltage, V_{dc2} (5 V/div. and 20ms/div) and (2) - charging current, I_{dc2} (500 mA/div. and 20 ms/div) at 269 rpm.

The average voltage V_{dc2} is 24.6 V, and the average current I_{dc2} is 1.65 A. Therefore, the output active power is 40.6 W, and the system efficiency is 81.2% (boost converter and rectifier). Increased efficiency and machine power factor are expected for high power prototypes.

Fig. 10 shows the generated phase voltage and the line current for mechanical speed of 470 rpm. In this case the boost converter is off.

For 470 rpm, the rms phase voltage is 13.33 V. The rms line current is 11.73 A. Therefore the total input apparent power is 464 VA and the input active power is 444 W. These values determine the operation of the machine for power factor of 0.95.

Fig. 11 shows the battery bank voltage V_{dc2} and charging current I_{dc2} for mechanical speed of 470 rpm. One can see that the average voltage V_{dc2} is 28.8 V. The average current I_{dc2} through the batteries is 13.8 A and the total active power is 397 W. Thus, the system efficiency (boost converter and rectifier) is 89%.

Fig. 12 shows the output power versus mechanical speed curves (simulated and experimental). The curves are similar, mainly when the processed power is greater that 300 W.

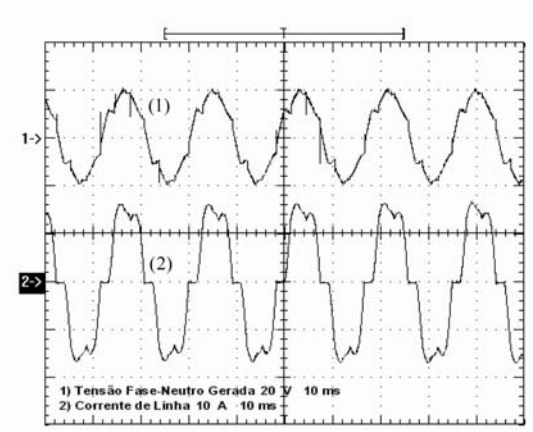

Fig. 10. (1) – Phase voltage (20 V/div. and 10 ms/div) and (2) -line current (10 A/div. and 10 ms/div) at 470 rpm.

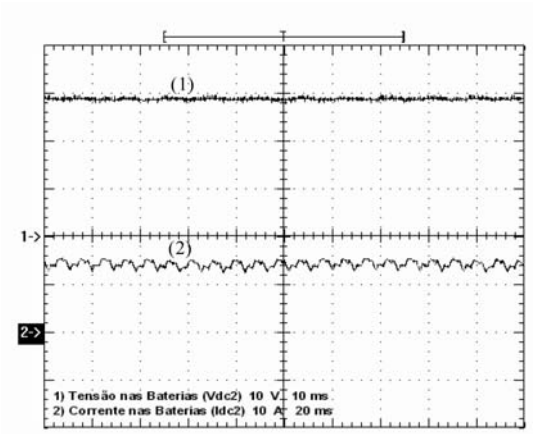

Fig. 11. (1) – Battery bank voltage, V_{dc2} (10 V/div. and 10 ms/div) and (2) - charging current, I_{dc2} (10 A/div. and 20 ms/div) at 470 rpm.

Fig. 13 shows the efficiency curve. The efficiency shown in the graph only considers the converters involved in the system. The internal losses of the machine are not considered. Fig. 14 shows the power factor of the permanent magnet synchronous generator as a function of the processed power.

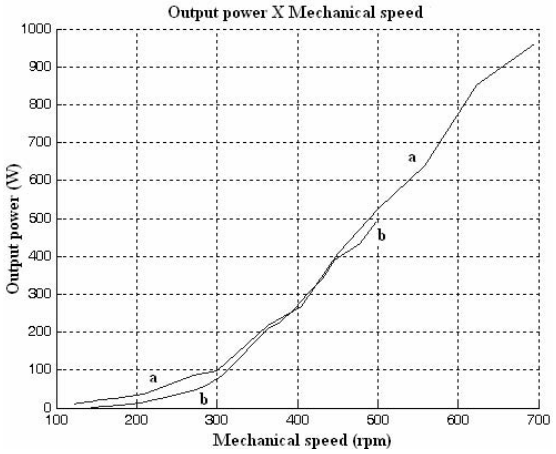

Fig. 12. Output power versus mechanical speed (a - simulated, b - experimental).

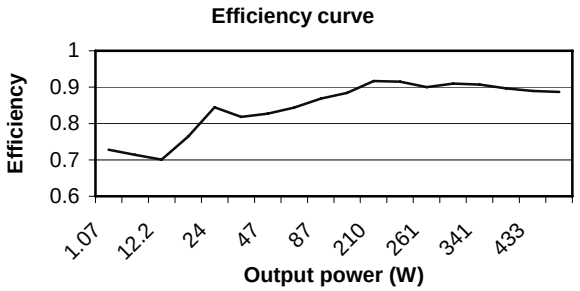

Fig. 13. Efficiency curve.

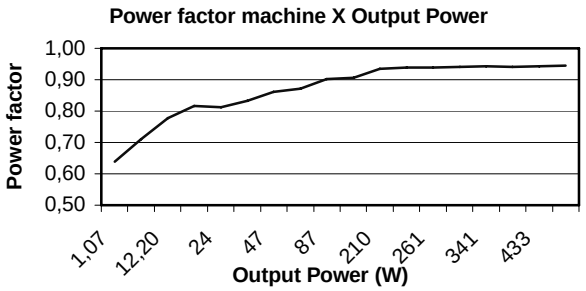

Fig. 14. Power factor machine versus output power.

VI. CONCLUSIONS

A new topology applied in small size wind generator systems for charging batteries has been proposed. A complete simulation of the system has been performed and validated through the comparison between experimental and manufacturer results (see Fig. 5).

The main characteristic of the new system is the exploitation of the available wind energy at low speeds in an optimum operating point (MPPT) without compromising the efficiency at higher wind speeds. Then, the auxiliary converter can be designed only for a given range with reduced overall cost. The example presented here (0-70 W) is according to the manufacturer specifications, but it can be extended by modifying some specifications of the generator.

Another improvement of the system is the charging controller implementation, which determines the increase of useful life of batteries. Other protection strategies have been implemented (limitation of the voltage and current charging), causing a considerable improvement to the battery charging system.

ACKNOWLEDGEMENT

The authors acknowledge FUNCAP and FINEP for the financial support; ENERSUD for the technical support and donation of the wind turbine; and the members of the Group of Energy Processing and Control (GPEC) for the friendship and overall support.

REFERENCES

[1] www.enersud.com.br, access in 21/10/2006, 10:40 AM.

[2] B.J. Chalmers; A.M. Green; A.B.J. Reece; A.H. Al-Badi, "*Modeling and Simulation of the Torus Generator*", IEE proceedings Electric power applications, 1997, vol. 144, n°6, pp. 446-452.

[3] A.H. Al-Badi and A. Gastli, "*MATLAB and PSPICE Dynamic Model of Axial-Field Permanent-Magnet.*", Department of Electrical Engineering, College of Engineering, Sultan Qaboos University, SQU Journal for Scientific Research – Science and Technology, 2002, Volume 7, part 1, pp. 109-121.

[4] N. Tomohiko; M. Shigeo; S. Masayuki; T. Yoji, "*Optimum Control of IPMSG for Wind Generation System*", Department of Electrical and Electronic Systems Osaka Prefecture University. (Presented PCC-Osaka 2002), pp. 1435-1440.

[5] Shigeo Morimoto, Hideaki Nakayama, Masayuki Sanada, Yoji Takeda. *"Sensorless Output Maximization Control for Variable-Speed Wind Generation System Using IPMSG"*, Industry Applications Conference, 2003. 38th IAS Annual Meeting IEEE. Vol. 3. pp.:1464-1471.

[6] Donald S. Zinger, Eduard Muljadi, Andrew Miller, *"A Simple Control Scheme for Variable Wind Turbines"*, IAS'96 Conference Record of the IEEE Industry Applications Conference 31st IAS Annual Meeting, 1996.

[7] Raju, A.B., Chatterjee, K., Fernandes, B.G., "A simple Maximum Power Point Tracker for Grid Connected Variable Speed Wind Energy Conversion System with Reduced Switch Count Power Converters", in IEEE 34th Annual Power Electronics Specialist Conference, PESC '03, Vol. 2, 15-19 June, 2003, pp. 748-753.

[8] Raju, A.B., Chatterjee, K., Fernandes, B.G., "A UPF power conditioner with maximum power point tracker for grid connected variable speed wind energy conversion system", in First International Conference on Power Electronics Systems and Applications, 2004, 9-11 Nov. 2004, pp.107-112.

[9] Song, S., Kang, S., Hahm, N., "Implementation and Control of Grid Connected AC-DC-AC Power Converter for Variable Speed Wind Energy Conversion System", in Eighteenth Annual IEEE Applied Power Electronics Conference and Exposition, 2003. APEC '03, Vol. 1, 9-13 Feb., 2003, pp. 154-158.

[10] Tafticht, T., Agbossou, K., Chériti, A., Doumbia, M.L., "Ouput Power Maximization of a Permanent Magnet Synchronous Generator Based Stand Alone Wind Turbine", in IEEE International Symposium on Industrial Electronics, ISIE 2006, July 9-12, Montreal, Canada, pp. 2412-2416.

[11] Z. Chen, E. Spooner, "Wind Turbine Power Converters: A Comparative Study", Power Electronics and Variable Speed Drives, 21-23 September 1998, Conference Publication No. 456, IEE 1998.